

Important Notice to Authors

Attached is a PDF proof of your forthcoming article in Optics Letters. The article Manuscript ID is 494189. *No further processing of your paper will occur until we receive your response to this proof.*

Note: *Excessive proof corrections submitted by the author can result in significant delays to publication. Please include only essential changes that might be needed to address any shortcomings noticed in the proof-preparation process.*

Author Queries

Please answer these queries by marking the required corrections at the appropriate point in the text or referring to the relevant line number in your PDF proof.


Q1	The funding information for this article has been generated using the information you provided to us at the time of article submission. Please check it carefully. If any information needs to be corrected or added, please provide the full name of the funding organization/institution as provided in the Crossref Open Funder Registry (https://search.crossref.org/funding).
----	--

Other Items to Check

- Please note that the original manuscript has been converted to XML prior to the creation of the PDF proof, as described above. The PDF proof was generated using LaTeX for typesetting. The placement of your figures and tables may not be identical to your original paper.
- Please carefully check all key elements of the paper, particularly the equations and tabular data.
- Author list: Please make sure all authors are presented, in the appropriate order, and that all names are spelled correctly.
- If figures need to be replaced because of accuracy or clarity concerns, please upload each revised figure as an individual PDF at the desired final size. In your corrections, please describe briefly what in the figure(s) has been changed.

Optics Letters

Wide-field probing of silica laser-induced damage precursors by photoluminescence photochemical quenching

Yoonsoo Rho, Christopher F. Miller, Robin E. Yancey, Ted A. Laurence, Christopher W. Carr, and Jae Hyuck Yoo* 

Physical and Life Sciences and NIF & Photon Sciences, Lawrence Livermore National Laboratory, Livermore, California 94550, USA

*yoo5@llnl.gov

Received 28 April 2023; revised 6 June 2023; accepted 9 June 2023; posted 14 June 2023; published 00 xxxxxx 0000

We describe a wide-field approach to probe transient changes in photoluminescence (PL) of defects on silica surfaces. This technique allows simultaneous capture of spatially resolved PL with spontaneous quenching behavior. We attribute the quenching of PL intensity to photochemical reactions of surface defects and/or subsurface fractures with ambient molecules. Such quenching curves can be accurately reproduced by our theoretical model using two quenchable defect populations with different reaction rates. The fitting parameters of our model are spatially correlated to fractures in silica where point defects and mechanical stresses are known to be present, potentially indicating regions prone to laser-induced damage growth. We believe that our approach allows rapid spatial resolved identification of damage prone morphology, providing a new pathway to fast, non-destructive predictions of laser-induced damage growth.

<https://doi.org/10.1364/OL.494189>

One of the major obstacles in the development of high-power and high-energy laser systems is laser-induced damage under illumination of sub-bandgap light. Initiated surface flaws on silica surfaces are significantly more vulnerable to damage growth by subsequent laser pulse trains at much lower fluences than the pristine surface damage threshold [1]. Substantial efforts have been made to improve the damage threshold by surface polishing [2], chemical etching of the surface [3], CO₂ laser annealing [4], and bulk annealing [5]. Such mitigation strategies have revealed that subsurface fractures and electronic defects are two significant laser-induced damage growth precursors in a pure silica sample. Those defect precursors increase absorption of subsequent pulses by simultaneously generating molten particles and ejecta, exponentially expanding the damage sites [6,7]. Similarly, surface flaws with a larger effective circular diameter (ECD) tend to grow at lower fluence [8,9], presumably due to the larger volume of structural defects and mechanical stresses formed in the subsurface. Although the ECD provides a simple and fast screening metric for damage site growth susceptibility, sites with similar ECD often show distinctly different probabilities for growth [10,11]. This suggests that damage site

morphology and quantity/density of electronic defects are also crucial in determining a site's growth susceptibility [12].

Studies of confocal time-resolved PL showed that quasi-continuum photoluminescence (QC-PL) with a broad distribution of lifetimes (~10 ps to ~5 ns) are associated with regions that undergo laser-induced damage [13,14]. QC-PL typically exhibits a broad and redshifted PL peak, attributed to a high density of defects [13,14] that may include the oxygen deficient center (ODC), non-bridging oxygen hole center (NBOHC), and unpaired dangling bond (\dot{E}), forming densely packed intermediate states with a broadened electronic energy structure. Subsequent chemical etching or annealing processes readily remove the QC-PL components, suggesting their correlation with the subsurface defects within few hundreds of nm depth [3,5]. Meanwhile, QC-PL from silica defects often present spontaneous bleaching upon laser illumination [14], indicating susceptibility to photochemistry. Previous studies showed that quenching of redshifted PL peaks at a surface flaw can be ascribed to neutralization of the E' defect by interstitial O₂⁻ ions [15,16]. Also, water content can passivate ODC and E' defects [17] as well as create NBOHC defects [18] in silica, potentially altering transient PL intensity. Such rich photochemical properties of silica suggest that the quenching dynamics of PL may serve as a spectral fingerprint for the local morphology of defects and their physicochemical properties, potentially predicting laser damage growth.

Here we introduce a wide-field PL method for studying local photochemical properties of defects in silica. The volatile dynamics in silica PL can be captured as a two-dimensional image stream, allowing fast probing of a damage site. Our theoretical model and fitting parameters to the PL quenching are well suited to measure the local morphology of a damage site, possibly showing a correlation to damage growth behavior by a subsequent laser pulse.

A single UV nanosecond pulse ($\lambda \sim 355$ nm, 5 ns) initiated surface flaws on silica surface (Corning 7980) at an energy density of 25 J/cm² with ECD in few tens of μ m [19], as shown in the laser confocal microscopy image (VK-X3000, Keyence) [Fig. 1(b)]. For wide-field PL probing [Fig. 1(a)], a 2.35-eV (532 nm) continuous wave (CW) laser was used (1

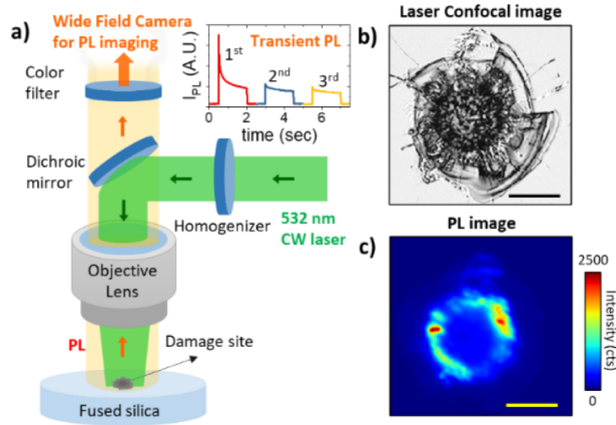


Fig. 1. (a) Schematic of wide-field PL dynamic imaging setup and the transient PL intensity by laser illumination at the surface flaws. (b) Laser confocal image and (c) time-averaged wide-field transient PL image of a silica damage site. The scale bars indicate 10 μm .

W, unless otherwise specified) for excitation, and a homogenizer (HM-201-Q-Y-A, Holo/Or) created a spatially uniform laser focal spot in a square shape on the sample surface (20 $\mu\text{m} \times 20 \mu\text{m}$) when coupled with an objective lens. A dichroic mirror reflected the laser beam to the sample, while transmitting the generated PL signal to a cooled CMOS camera (Sona, Andor) after passing through multi notch filters (NF533-17, Thorlabs). A motorized XY stage (ANT130XY, Aerotech) translating the sample automatically located a damage site with predefined coordinates, allowing rapid inspection of many damage sites.

Typical damage sites displayed strong PL intensities at relatively low energy ($\sim 2.7 \text{ eV}$) with a broad spectrum representing the QC-PL signatures due to high defect density [13,14]. Furthermore, spontaneous quenching upon CW laser illumination within a few 10^{-2} seconds was noted [inset of Fig. 1(a), and Fig. 2(a)], while subsequent immediate laser illumination could not reproduce a similar level of quenching [inset of Fig. 1]. This indicates that measuring PL by point laser scanning may affect the quenching dynamics of surrounding regions. Thus, the wide-field approach allows capturing the volatile early quenching dynamics of PL in a two-dimensional image stream (12 ms for each frame) [Fig. 1(c)] from the entire region of an as-initiated damage site [Fig. 1(b)]. We note that such quenching behavior can be reproduced after a few weeks of storage at ambient condition. Recovery of PL behavior on this time scale is consistent with a photochemical reaction with ambient molecules. Previous studies showed that O_2^- ions neutralize E' defects [15,16], decaying PL intensity. Also, water molecules at silica surfaces can remove or create defect centers [17,18]. In addition to silica, the ambient dependent PL intensity change has been reported for other oxide materials including TiO_2 , ZnO , MgO , and perovskite where the photoexcited electrons at the surface of those materials can induce reversible absorption and desorption of electron-acceptor molecules followed by healing of point defects [20].

Based on the above observations, we propose a theoretical model assuming healing of radiative point defects in silica with two different quenching rates. The openness of subsurface fractures and cracks may affect the accessibility of the ambient molecules to these point defects, resulting in fast (F) and slow

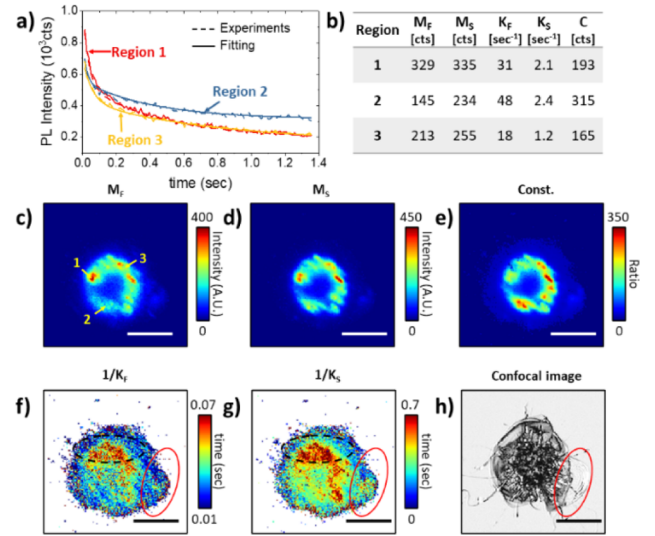


Fig. 2. (a) Transient PL profile extracted from the regions 1, 2, and 3 shown in panel (c) and their corresponding fitting curves based on Eq. (4). (b) Fitting parameters for the curves in panel (a). (c)–(g) Spatial plots of fitting parameters showing (c) M_F , (d) M_S , (e) C , (f) $1/k_F$, and (g) $1/k_S$. (h) Laser confocal image showing morphology of the damage site. The red ellipses in panels (f)–(h) indicate a fractured shell, showing an example of correlation between PL fitting and topography signatures. The black dashed ellipses in panels (f)–(g) correspond to the region 3 in panel Fig. 3(c). The scale bars are 10 μm .

(S) relaxation rates in their PL dynamics. After consuming all accessible defects by ambient molecules, the residual PL components can be attributed to a non-quenchable defect $[D]_n$. Then, the transient defect density $[D]$ upon illumination of laser with intensity L can be described by a diffusion model with quenching rate $k(L)$:

$$\frac{d[D]_F}{dt} = -k_F(L)([D]_F - [D]_{n,F}), \quad (1)$$

$$\frac{d[D]_S}{dt} = -k_S(L)([D]_S - [D]_{n,S}). \quad (2)$$

The equation describes the dynamically reducing PL active point defect by photochemical reactions with ambient molecules at rate k of surface flaws. Then, the observable PL intensity can be described by a function of defect density $[D]$ and laser intensity L . Previous studies revealed that PL from semiconductors and amorphous materials can have exponential law α to L , depending on their origin of radiative recombination rate [21]:

$$I_{PL} \sim ([D]_F + [D]_S)L^\alpha, \quad (3)$$

with Eqs. (1) and (2), gives

$$I_{PL} \sim M_F e^{-k_F(L)t} + M_S e^{-k_S(L)t} + C, \quad (4)$$

where $M_F = ([D]_{i,F} - [D]_{n,F})L^\alpha$, $M_S = ([D]_{i,S} - [D]_{n,S})L^\alpha$ are the fast and slow local quenchable defect density, respectively, and $C = ([D]_{n,F} + [D]_{n,S})L^\alpha$ is the non-quenchable defect density, indicating fully quenched behavior. Here, $[D]_i$ indicates the initial defect density at time zero before any quenching event occurs. Equation (4), with M_F , M_S , k_F , k_S , and C as fitting parameters, explains the observed quenching behavior (Fig. 2).

We performed wide-field PL imaging on a damage site. In the laser confocal image, a molten pool with smooth and small

features is clearly seen at the center, while cracks and fractured shell are clearly visible at the periphery [Fig. 2(h)]. Intensity curves fit using Eq. (4) follow the experimentally obtained PL profiles from regions 1, 2, and 3 indicated in Fig. 2(c) [Fig. 2(a)]. The fitting parameters are tabulated in Fig. 2(b), representing the distinctly different local PL dynamics in a micron-scale spatial resolution at a single surface flaw. In most cases, the fast quenchable defects exhibit approximately an order of magnitude faster rate than that of the slow quenchable defects. Regions 1 and 3 show strong PL intensity with similar values for fast and slow quenchable defects (e.g., $M_F \approx M_S$), while their quenching rates are relatively small for both types of defects. However, region 2 shows relatively weak PL intensity but a distinctly different ratio of fast and slow quenchable defects density (e.g., $M_F < M_S$), suggesting slow quenchable defects dominate the photochemical reaction dynamics at this region. Such contrast in fitting parameters for slow and fast quenchable defects may allow for the prediction of damage growth susceptibility, which is discussed later. It should also be noted that wide-field PL imaging can accurately represent topographic features of damage sites as shown in both $1/k_F$ and $1/k_S$ metrics [Figs. 2(f) and 2(g)]. Fittings were performed on spatial locations with PL intensity higher than 10 counts in the first captured image, and this simple screening identifies the fractured shell and cracks shown in laser confocal images [indicated by the red ellipses in Figs. 2(f)–2(h) and a combined image of Figs. 2(e) and 2(h) is available in Fig. S1).

The input laser power dependent study showed that the power exponent law α in $M_F = L^\alpha$ and $M_S = L^\alpha$ are 0.22 and 0.26, respectively (Fig. S3a). Such values indicate that the donor–acceptor pair recombination by densely packed defects are dominant mechanisms in our observed PL dynamics [21] (Supplement 1). Meanwhile, the quenching rates k_F and k_S show a power dependence with the Arrhenius equation ($\log(k) \propto 1/L$) at lower laser power (<0.5 W), representing a reaction limited behavior (Fig. S3b). At higher laser power (>0.5 W), reaction rates show a non-varying trend, representing a mass transport limited behavior, consistent with the reaction-diffusion limited model which are commonly used in thermally activated solid–gas reaction systems [22,23].

We investigated potential relations of the fitting parameters to the laser induced damage growth susceptibility. A subsequent UV nanosecond laser pulse can induce additional damage growth of already existing surface flaws in silica at much lower energy density (8 J/cm^2) than damage initiation in pristine silica (25 J/cm^2). The high local optical absorption at the preformed mechanical cracks and induced stresses significantly lower the damage threshold at the surface flaws. Near 50% of surface flaws showed more than 1% of ECD changes ($\text{ECD}_{\text{Pre}} - \text{ECD}_{\text{Post}}/\text{ECD}_{\text{Pre}}$) after the damage growth experiment. The pre- and post-laser confocal images show local morphology changes after laser induced damage growth [Figs. 3(d), 3(h), 3(i)]. Here, we propose two metrics [e.g., $C/(M_F + M_S + C)$ and M_S/M_F] that may reflect subtle physical mechanisms related to the laser induced damage growth. The first metric $C/(M_F + M_S + C)$ corresponds to the fraction of non-quenchable defect density C to the total PL-active defect density ($M_F + M_S + C$). The second metric, M_S/M_F , is a ratio between the fast and the slow quenchable defects, representing dominance of the slow quenchable defects. We found that these metrics represent the microscopic features of the damage site (Fig. S2), and the regions with high values of these metrics can

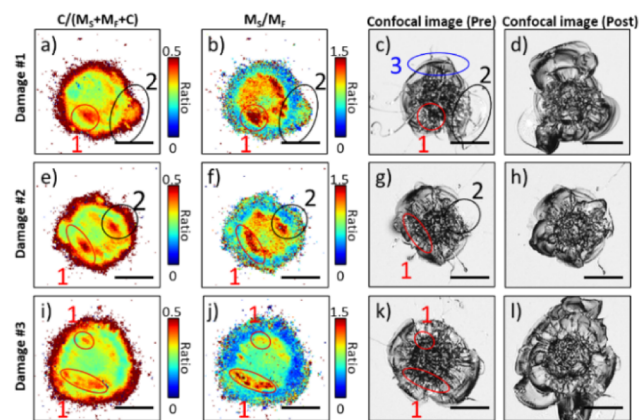


Fig. 3. Plots of $C/(M_F + M_S + C)$ and M_S/M_F derived from wide-field dynamic PL images juxtaposed with laser confocal images taken before (pre) and after (post) the second laser shot for laser induced damage growth. The ellipses labeled with 1, 2, and 3 indicate regions correlated with different types of potential damage precursors. Three damage sites were used: (a)–(d) damage site 1 (the same damage site shown in Fig. 2), (e)–(h) damage site 2, and (i)–(l) damage site 3. The scale bars are $10 \mu\text{m}$.

potentially be prone to damage growth (Region 1 in Fig. 3). These are closely related to the topographic features of the surface flaws. The slow quenchable and non-quenchable defects likely locate in the subsurface fractures in a deeper region, whereas the fast quenchable defects present at the surface that is easily accessible to the ambient molecules. Previous studies showed that the surface flaws with larger ECD have lower damage thresholds mainly due to the subsurface flaws that extend deeper into the surface [8,9]. Those larger fractures possess more stresses and densification [12], which are vulnerable to stress driven crack propagation [24]. Also, field intensification is more probable at the wider fractures as its gap size becomes closer to the wavelengths [12,25]. For the region 2 in Fig. 3, the presence of a fractured shell manifested by the non-circularity in the contour of PL images tends to be a damage growth precursor, owing to the reduced mechanical strength [12,26]. Finally, some of the damage growth is not well correlated with either metric (Region 3 in Fig. 3). These regions correlate with a long quenching time constant ($1/k_F$ and $1/k_S$) indicated by black dashed ellipses in Fig. 2(f) and (g), suggesting that the quenching rates of both quenchable defects are important.

In summary, we show that wide-field dynamic PL imaging can capture photochemical quenching of PL of surface flaws in silica. The use of wide-field probing can capture the volatile dynamics of PL. The fitting parameters with our suggested model can be well correlated with the local morphology of surface flaw, showing potential use of laser damage growth prediction.

Funding. Lawrence Livermore National Laboratory (22-ERD-003).

Acknowledgments. This work was performed under the auspices of the U.S. Department of Energy by Lawrence Livermore National Laboratory under Contract DE-AC52-07NA27344.

Disclosures. The authors declare no conflicts of interest.

Data availability. Data are available from the authors upon reasonable request.

Supplemental document. See Supplement 1 for supporting content.

REFERENCES

1. B. C. Stuart, M. D. Feit, S. Herman, A. M. Rubenchik, B. W. Shore, and M. D. Perry, *Phys. Rev. B* **53**, 1749 (1996).
2. B. Bertussi, J.-Y. Natoli, and M. Commandre, *Opt. Commun.* **242**, 227 (2004).
3. P. E. Miller, J. D. Bude, T. I. Suratwala, N. Shen, T. A. Laurence, W. A. Steele, J. Menapace, M. D. Feit, and L. L. Wong, *Opt. Lett.* **35**, 2702 (2010).
4. R. N. Raman, M. J. Matthews, J. J. Adams, and S. G. Demos, *Opt. Express* **18**, 15207 (2010).
5. N. Shen, P. E. Miller, J. D. Bude, T. A. Laurence, T. I. Suratwala, W. A. Steele, M. D. Feit, and L. L. Wong, *Opt. Express* **51**, 121817 (2012).
6. N. Shen, J. D. Bude, and C. W. Carr, *Opt. Express* **22**, 3393 (2014).
7. C. W. Carr, J. D. Bude, and P. DeMange, *Phys. Rev. B* **82**, 184304 (2010).
8. R. A. Negres, M. A. Norton, D. A. Cross, and C. W. Carr, *Opt. Express* **18**, 19966 (2010).
9. R. A. Negres, Z. M. Liao, G. M. Abdulla, D. A. Cross, M. A. Norton, and C. W. Carr, *Appl. Opt.* **50**, D12 (2011).
10. J. Wong, J. L. Ferreira, E. F. Lindsey, D. L. Haupt, I. D. Hutcheon, and J. H. Kinney, *J. Non-Cryst. Solids* **352**, 255 (2006).
11. G. Hu, Y. Zhao, D. Li, Q. Xiao, J. Shao, and Z. Fan, *Surf. Interface Anal.* **42**, 1465 (2010).
12. R. N. Raman, R. A. Negres, M. J. Matthews, and C. W. Carr, *Opt. Mater. Express* **3**, 765 (2013).
13. T. A. Laurence, J. D. Bude, N. Shen, T. Feldman, P. E. Miller, W. A. Steele, and T. Suratwala, *Appl. Phys. Lett.* **94**, 151114 (2009).
14. T. A. Laurence, J. D. Bude, N. Shen, W. A. Steele, and S. Ly, *J. Appl. Phys.* **115**, 083501 (2014).
15. J. Fournier, J. Neauport, P. Grua, E. Fargin, V. Jubera, D. Talaga, and S. Jouannigot, *Appl. Phys. Lett.* **100**, 114103 (2012).
16. L. Skuja, *J. Non-Cryst. Solids* **179**, 51 (1994).
17. K. Kokura, M. Tomozawa, and R. K. MacCrone, *J. Non-Cryst. Solids* **111**, 269 (1989).
18. S. MuneKuni, T. Yamanaka, Y. Shimogaichi, R. Tohmon, Y. Ohki, K. Nagasawa, and Y. Hama, *J. Appl. Phys.* **68**, 1212 (1990).
19. M. J. Runkel, A. K. Burnham, D. Milam, W. D. Sell, M. D. Feit, and A. M. Rubenchik, in *Laser-Induced Damage in Optical Materials: 2000*, Vol. 4347 (SPIE, 2001), pp. 359–372.
20. Z. Zhang and J. T. Yates, *Chem. Rev.* **112**, 5520 (2012).
21. T. Schmidt, K. Lischka, and W. Zulehner, *Phys. Rev. B* **45**, 8989 (1992).
22. S. Möller, A. Kreter, C. Linsmeier, and U. Samm, *Nucl. Mater. Energy* **1**, 1 (2015).
23. D. Hegemann, in *Comprehensive Materials Processing*, S. Hashmi, G. F. Batalha, C. J. Van Tyne, and B. Yilbas, eds. (Elsevier, 2014), pp. 201–228.
24. F. Dahmani, J. C. Lambropoulos, A. W. Schmid, S. Papernov, and S. J. Burns, *J. Mater. Res.* **14**, 597 (1999).
25. H. Wang, C. Wang, M. Zhang, E. Zheng, J. Hou, and X. Chen, *Appl. Opt.* **58**, 9839 (2019).
26. M. D. Feit and A. M. Rubenchik, in *Solid State Lasers for Application to Inertial Confinement Fusion: Second Annual International Conference*, Vol. 3047 (SPIE, 1997), pp. 971–977.